Journal of Zhejiang University-SCIENCE A (Applied Physics & Engineering) 2025 26(2):109-120
www.jzus.zju.edu.cn; www.springer.com/journal/11582
E-mail: jzus_a@zju.edu.cn

Research Article

https://doi.org/10.1631/jzus.A2300638

Structural optimization of the rotary valve in a two-stage Gifford-McMahon-type pulse-tube cryocooler working at liquid helium temperatures

Qinyu ZHAO[1], Jun CHENG[2], Yanrui ZHANG[2], Haoren WANG[2,3], Bo WANG[2]✉, Ruize LI[2,3], Hua ZHANG[1]✉, Zhihua GAN[2,3]

[1]*School of Energy and Power Engineering, University of Shanghai for Science and Technology, Shanghai 200093, China*
[2]*Key Laboratory of Refrigeration and Cryogenic Technology of Zhejiang Province, Hangzhou City University, Hangzhou 310015, China*
[3]*Key Laboratory of Refrigeration and Cryogenic Technology of Zhejiang Province, Zhejiang University, Hangzhou 310027, China*

Abstract: Gifford-McMahon-type pulse-tube cryocoolers (GM-PTCs) working at liquid helium temperatures are promising in quantum technology and cryogenic physics for their high reliability and minimal vibration. These features stem from the fact that there are no extra moving parts introduced into the system. The rotary valve is a key component in GM-PTCs that transfers the output exergy from the compressor to the cold head. Because a low Carnot efficiency of 1.58% is achieved at liquid helium temperatures, optimizing the rotary valve is crucial for improving the efficiency of GM-PTCs. In this regard, an exergy-loss analysis method is proposed in this paper to quantitatively obtain the leakage loss and viscosity loss of a rotary valve by experimental measurements. The results show that viscosity loss accounts for more than 97.5% of the total exergy loss in the rotary valve, and that it is possible to improve the structure of the rotary valve by expanding the flow area by 1.5 times. To verify the method, the cooling temperature and power of a remote two-stage GM-PTC were monitored, with original or optimized rotary valves installed. The experimental results show that compared to the original rotary valve, the optimized rotary valve can improve the cooling efficiency of a GM-PTC by 16.4%, with a cooling power of 0.78 W at 4.2 K.

Key words: Rotary valve; Exergy analysis; Liquid helium temperature; Gifford-McMahon-type pulse-tube cryocooler (GM-PTC); High efficiency

1 Introduction

Compared with Gifford-McMahon (GM) cryocoolers, Gifford-McMahon-type pulse-tube cryocoolers (GM-PTCs) have no moving parts at the cold end, and have inherently high reliability, long life, low vibration, and no electromagnetic interference (Ji et al., 2022; Kasai et al., 2022), making them a promising cooling source for applications such as the superconductive quantum interference device (SQUID), superconducting quantum chip cooling (Choi, 2022; Hollister et al., 2023), and particle physics (Alduino et al., 2019; The CUORE Collaboration, 2022). Although GM-PTCs have become mature commercial products (Bluefors, 2023b; SHI Cryogenics Group, 2023), they still have limitations in terms of low cooling capacity and efficiency (de Waele, 2011, 2012). The PT425 GM-PTC manufactured by Cryomech, for example, can provide a cooling capacity of 2.7 W at 4.2 K, but its relative Carnot efficiency is as low as 1.58% (Hao et al., 2022; Bluefors, 2023a). Therefore, improving the efficiency at liquid helium temperature is vital for the large-scale application of GM-PTCs (Wang and Gan, 2013; Lei and Xu, 2022).

The GM-PTC system consists of a compressor, distribution valve, and cold head. A series of theoretical studies have been carried out on the side with the cold head, including attempts to optimize the regenerator (Gan et al., 2009), pulse tube (Liang and de

✉ Bo WANG, wangbo@hzcu.edu.cn
Hua ZHANG, zhanghua@usst.edu.cn
Bo WANG, https://orcid.org/0009-0001-2483-5665
Hua ZHANG, https://orcid.org/0000-0002-0294-7981

Received Dec. 18, 2023; Revision accepted Mar. 25, 2024; Crosschecked Jan. 10, 2025

Waele, 2007), and phase shifters (Zhu et al., 2009) to improve efficiency. With regard to the compressor and distribution valves, many numerical investigations have been conducted with the help of Sage (Gedeon, 2014) and computational fluid dynamics (Karpenko and Bogdevičius, 2020), and a very limited number of studies have examined ways to measure the significant exergy losses suffered by the compressor and distribution valves of GM-PTCs (Liu et al., 2017).

The exergy loss of the compressor in a Stirling-type pulse-tube cryocooler is about 20% to 30% (Radebaugh et al., 2002; Tanaeva et al., 2006), but the exergy loss of the compressor in a GM-PTC uses up about 50% of the input electrical power (Liu et al., 2017). The compressors applied in GM-PTCs are commercial products, making it very difficult to improve exergy efficiency and keep costs low (Hitachi, 2023). In addition, there is still a 30% exergy loss in the distribution valves of the GM-PTC, according to the simulation conducted by Liu et al. (2017). Therefore, optimization of the distribution valves is one of the most essential research avenues for improving the cooling efficiency of GM-PTCs (Karpenko et al., 2023; Zhao et al., 2023).

The rotary valve and solenoid valve are two typical distribution valves for GM-PTCs. Since the empirical coefficients of each distribution valve need to be calibrated via experiments, the effect of the structure and timing of these two valves on the cooling performance of GM-PTCs is studied mostly by experimental investigations, as summarized below.

Many studies have been conducted to investigate the effect of the structure of distribution valves on GM-PTCs. Thummes et al. (1995) coupled a GM-PTC with a rotary valve and a series of needle valves to change the pressure-wave form into the cold head and investigated the effect of the wave forms on cooling performance. The results showed that a pressure-wave form with long dwell times at peak pressures resulted in a lower cooling temperature of 61 K compared to the 69 K obtained by a sine pressure-wave form. Wang et al. (2010) adopted three solenoid valves and a rotary valve as the distribution valves for a GM-PTC. When the number of solenoid valves increased from one to three, the hot-end pressure ratio rose from 1.71 to 1.94, achieving a lower no-load cooling temperature between 15.7 K and 14.4 K. Since the flow area of the solenoid valves was much smaller than that of the rotary valve, a higher hot-end pressure ratio of 2.19 was obtained when replacing the three solenoid valves with a rotary valve, achieving a lower no-load cooling temperature of 12.4 K.

With regard to the effect of the timing of distribution valves on cryocooler performance, Zhu et al. (1998) investigated the effect of the length of the waiting time (i.e., the period when the high-pressure valve and low-pressure valve are both closed) of solenoid valves on an orifice pulse-tube cryocooler by conducting numerical simulations and experiments. The numerical results showed that when the waiting time increased from 0 to 1/4 cycle, the no-load cooling temperature of the cryocooler decreased. Meanwhile, the experiments showed that when the waiting times were 1/360 cycle and 1/4 cycle, the no-load cooling temperature of the cryocooler was 45.1 K and 40.3 K, respectively. Qiu and Thummes (2002) conducted an experimental investigation on the ratio of exhaust time to intake time in the range of 1.05 to 1.41 for a two-stage GM-PTC working at liquid helium temperatures. The optimum ratio depended on the input power of the compressor. When the input power of the compressor was low (1.7 kW), a smaller ratio (1.05) achieved a higher mass flow rate to the cold head and allowed the GM-PTC to reach a maximum cooling power of 202 mW at 4.2 K. When the input electric power of the compressor was high enough (6 kW), a larger ratio of 1.3 achieved a maximum cooling power of 500 mW at 4.2 K.

From the above literature survey, it is clear that most studies have concentrated on studying the feasibility of distribution valves by comparing the effects of different structures and valve timing on the performance of cryocoolers, but very few studies have focused on analyzing exergy loss in distribution valves. In this paper, we propose a test method for assessing the exergy loss, including the leakage loss and viscosity loss, in a rotary valve. With the help of this method, the distribution of leakage loss and viscosity loss in a rotary valve under different operating conditions can be obtained and analyzed, providing guidance to optimize the rotary valve by expanding its flow area by 1.5 times. To verify the method, we monitored the cooling temperature and power of a remote two-stage GM-PTC with original or optimized rotary valves installed. The experimental results show that compared to the original rotary valve, the optimized rotary valve can improve cooling efficiency by 16.4%, with a cooling power of 0.78 W at 4.2 K.

2 Experimental test of exergy loss from a rotary valve

2.1 Tested rotary valve

The rotary valve, consisting of a suction valve and discharge valve, is a distribution valve that opens and closes periodically according to specific timing. As shown in Fig. 1, when the discharge valve is opened, the cold head is connected to the high-pressure gas source for pressurization (the discharge period). When the suction valve is opened, the cold head is connected to the low-pressure gas source for depressurization (the suction period). Normally, the suction and discharge valves are not open at the same time. When they are closed at the same time, it is called the quiet period.

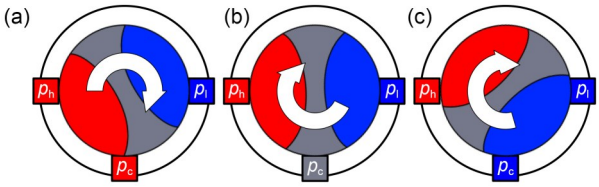

Fig. 1 Schematic diagram of three steps for a working rotary valve: (a) discharge period; (b) quiet period; (c) suction period. p_h is the high pressure; p_l is the low pressure; p_c is the pressure in the load (i.e., reservoir and cold head)

Fig. 2 displays the basic structure of the tested rotary valve. Inside the rotary valve, there is a stator and a rotor. The valve spool has a symmetrical arrangement to eliminate the unbalanced differential pressure exerted on the rotor, and there is a dead space between the rotor and bushing; therefore, there is no friction in this rotary valve caused by the asymmetrical differential pressure. The stator has two orifices with an equivalent flow area of 16 mm^2, to let the helium gas in and out of the cold head. The rotor has a groove connecting the high-pressure and low-pressure chambers of the compressor. By means of the matching relationship between the stator and rotor, the rotary valve changes the direct current (DC) flow into low-frequency alternating flow to drive the cold head of a GM-PTC. Thus, to improve the efficiency of GM-PTCs, clarification of exergy loss in the rotary valve is of great value.

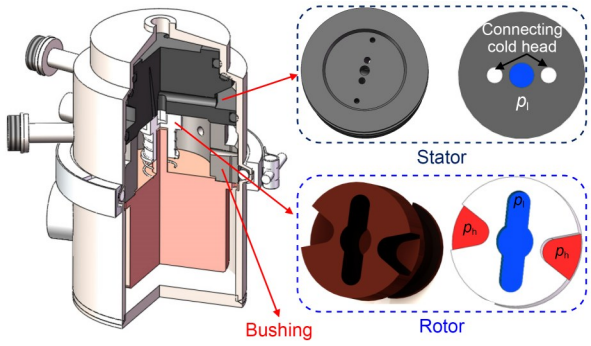

Fig. 2 Basic structure of the tested rotary valve

2.2 Exergy loss test of a rotary valve

The exergy loss generated in a rotary valve consists of leakage loss and viscosity loss (Zhao et al., 2023):

$$\dot{E}=\dot{E}_{\mathrm{leak}}+\dot{E}_{\mathrm{fric}}, \tag{1}$$

where $\dot{E}$ is the total exergy loss, $\dot{E}_{\mathrm{leak}}$ is the exergy loss caused by gas leakage, and $\dot{E}_{\mathrm{fric}}$ is the exergy loss caused by flow resistance.

2.2.1 Leakage loss

The exergy loss caused by gas leakage between the high-pressure and low-pressure gas chambers is called leakage loss, and is expressed as follows:

$$\dot{E}_{\mathrm{leak}}=\frac{1}{\tau}\int_0^{\tau}(g_{\mathrm{h}}-g_{\mathrm{l}})\dot{m}_{\mathrm{leak}}\mathrm{d}t, \tag{2}$$

where subscripts h and l denote the high pressure and low pressure corresponding to the suction and exhaust processes, respectively. g is the specific Gibbs free energy, τ represents the period of one cycle, t is the time, and $\dot{m}_{\mathrm{leak}}$ denotes the mass flow rate of the leaked gas.

The mass flow rate of gas leakage in Eq. (2), expressed by Eq. (3) (Zhu et al., 1997), is dependent on the pressure difference (Δp) between the high-pressure (p_{h}) and low-pressure (p_{l}) gas sources and on the leakage coefficient:

$$\dot{m}_{\mathrm{leak}}=K\sqrt{\rho_{\mathrm{l}}(p_{\mathrm{h}}-p_{\mathrm{l}})}=K\sqrt{\rho_{\mathrm{l}}\Delta p}, \tag{3}$$

where ρ_{l} is the density of the gas at low pressure, and K is the leakage coefficient. The leakage coefficient is a characteristic factor of a rotary valve that changes with pressure differences and operating frequencies. It should be noted that the leakage mass flow rate $\dot{m}_{\mathrm{leak}}$ cannot be directly measured when the rotary valve is connected to a compressor and a cold head. Therefore, $\dot{m}_{\mathrm{leak}}$ should be calibrated by the leakage

coefficient K and pressure difference Δp in the calculation of $\dot{E}_{\text{leak}}$.

To calibrate the leakage coefficient of the rotary valve under various pressure differences and operating conditions, we established a test platform with the positions of measuring mass flow rate and pressure, as shown in Fig. 3.

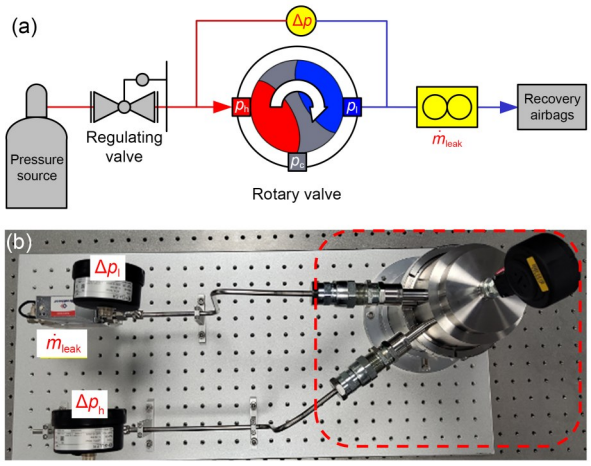

Fig. 3 Test platform for the leakage coefficient of rotary valve: (a) schematic diagram; (b) photograph

In the experimental system, two Keller LEO3 digital pressure gauges were utilized to test the pressure difference in Eq. (3), and a Bronkhorst F-201A flowmeter was applied to monitor the leakage mass flow rate $\dot{m}_{\text{leak}}$. Detailed information on the measured parameters is listed in Table 1.

It should be noted that the measured pressure differences take into account the pressure drops along the way of valve measuring connectors. Compared to the large pressure difference inside the rotary valve, the pressure drops caused by the connectors can be neglected in the testing process. During testing of the leakage coefficients, the load side of the rotary valve was blocked by a self-sealing connector to force all the leaked gas to go through the flowmeter. When the rotary valve worked at a fixed operating frequency, the high-pressure gas was adjusted to the desired pressure with the regulating valve. The gas leaked from the high-pressure side of the rotary valve to the low-pressure side and then entered the recovery airbags.

In addition to recording the pressure differences and leakage mass flow rate with different frequencies, we monitored ambient temperatures to calculate the ρ_1 in Eq. (3), with the help of the database of National Institute of Standards and Technology (NIST), USA. After obtaining $\dot{m}_{\text{leak}}$, Δp, and ρ_1 at a fixed operating frequency (f), we calibrated the leakage coefficient K. Fig. 4a presents the changes in the leakage coefficient with pressure difference, with different operating frequencies in the range of 1.2 to 2.4 Hz.

When Δp changed from 0.6 MPa to 1.6 MPa, the relative change of K was less than 2%, indicating that

Table 1 Information on the parameters measured on the test platform for the leakage coefficient of rotary valve

Parameter	Symbol	Sensor	Range	Uncertainty
Differential pressure	Δp_h, Δp_l	Keller LEO3	0–3.0 MPa	±3 kPa
Mass flow rate for leakage test	$\dot{m}_{\text{leak}}$	Bronkhorst F-201A Flowmeter	0–80 L/min	±0.08 L/min

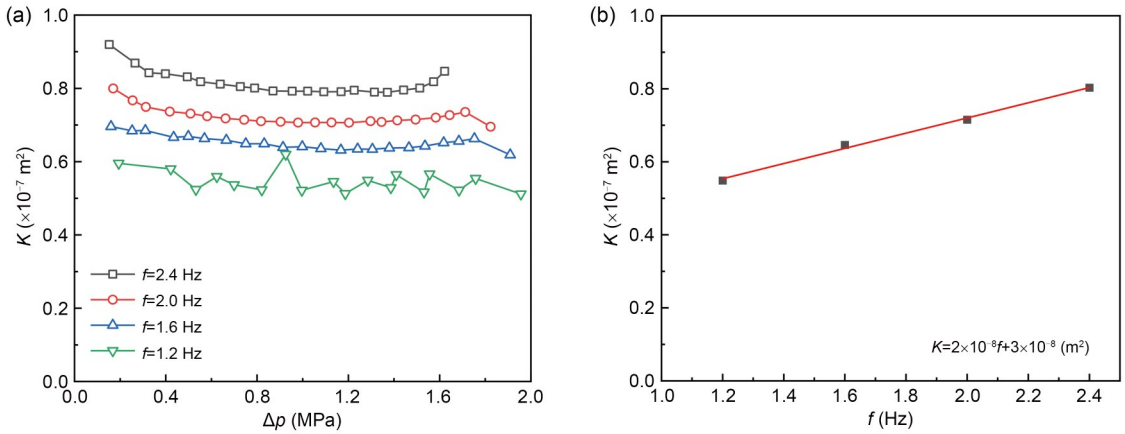

Fig. 4 Experimental results of the leakage coefficient for the rotary valve: (a) relationship between leakage coefficient and pressure difference with different operating frequencies; (b) linear fitting of leakage coefficient with operating frequency

K was only related to the operating frequency. The averaged leakage coefficient, after calculating an integral average of K from 0.6 MPa to 1.6 MPa at each point of operating frequency, is displayed in Fig. 4b. The analytical correlation between the leakage coefficient and operating frequency for the rotary valve can be obtained through the linear fitting.

2.2.2 Viscosity loss

Exergy losses caused by non-linear flow resistance of the nozzle in the discharge valve and suction valve are defined as follows:

$$\dot{E}_{\mathrm{fric,d}}=\frac{1}{\tau}\int_0^{\tau}(g_{\mathrm{h}}-g_{\mathrm{c}})\dot{m}\mathrm{d}t\ (\dot{m}>0), \tag{4}$$

$$\dot{E}_{\mathrm{fric,s}}=\frac{1}{\tau}\int_0^{\tau}(g_{\mathrm{c}}-g_{\mathrm{l}})|\dot{m}|\mathrm{d}t\ (\dot{m}<0), \tag{5}$$

where the subscript c represents the load (cold head or reservoir), subscripts d and s represent the discharge valve and suction valve, respectively, and $\dot{m}$ is the mass flow rate.

To assess the viscosity loss from the rotary valve under different operating conditions, we established the experimental platform shown in Fig. 5.

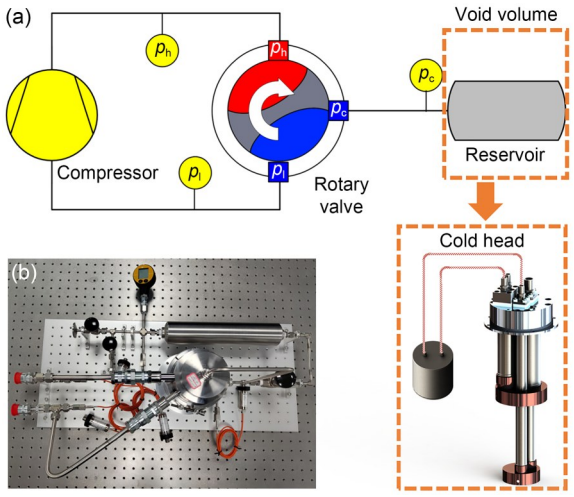

Fig. 5 Experimental platform used to assess viscosity loss in the rotary valve: (a) schematic diagram; (b) photograph

The suction and discharge valves in the tested rotary valve were connected to the high-pressure and low-pressure chambers in a scroll compressor (S603DH) manufactured by Hitachi, Japan, with a steady-state input electrical power of 6–7 kW. The load connected to the rotary valve was two constant-volume gas reservoirs (0.5 L and 2.0 L) maintained at ambient temperature by water cooling. These reservoirs represented the total void volume of the cold head of the GM-PTC rather than the void volume of a specific component such as the pulse tube or reservoir. Table 2 lists the information on the parameters measured on the experimental platform, presented in Fig. 5.

Table 2 Information on the parameters measured on the experimental platform shown in Fig. 5

Parameter	Symbol	Sensor	Range	Uncertainty
Electric power		DTSU5886	0–13.2 kW	±0.1 kW
Pressure oscillation	p_{h}, p_{l}, p_{c}	Keller M5HB	0–5.0 MPa	±5 kPa

Since the compressibility factor of helium at ambient temperature (about 300 K) is close to unity according to the NIST database, we next applied the ideal gas equation of state to describe the helium. It should be noted that the gas reservoir shown in Fig. 5 was utilized to measure the alternating mass flow rate through the rotary valve with the resistance and compliance (RC) load approach (Swift, 2002). Normally, the temperature of the gas reservoir is assumed to be constant in the RC load approach (Zhou and Matsubara, 1998). To keep the temperature of the gas reservoir as constant as possible during the compression and expansion process, the reservoir was placed in water which was controlled at 300 K by a thermostat with an uncertainty of 0.03 K. Assuming the isothermal process in the gas reservoir, the alternating mass flow rate can be expressed by:

$$\dot{m}=\frac{V_{\mathrm{res}}}{RT_0}\frac{\mathrm{d}p_{\mathrm{c}}}{\mathrm{d}t}, \tag{6}$$

where V_{res} is the volume of the reservoir, R is the gas constant of helium, and T_0 is the ambient temperature. In addition to accurately measuring the alternating mass flow rate, monitoring the high pressure and low pressure is essential in calculating the Gibbs free energy in Eqs. (4) and (5). Therefore, we used three Keller M5HB high-frequency pressure transducers (with an uncertainty of ±5 kPa), to monitor the high pressure (p_{h}) and low pressure (p_{l}), as well as the transient pressure in the gas reservoir (p_{c}) (Fig. 4).

Combined with Eqs. (4)–(6), the exergy loss of viscosity can be expressed as follows:

$$\dot{E}_{\mathrm{fric,d}}=\frac{V_{\mathrm{res}}}{RT_0}\int_{\min p_{\mathrm{c}}}^{\max p_{\mathrm{c}}}(g_{\mathrm{h}}-g_{\mathrm{c}})\,\mathrm{d}\,p_{\mathrm{c}}, \tag{7}$$

$$\dot{E}_{\mathrm{fric,s}}=\frac{V_{\mathrm{res}}}{RT_0}\int_{\min p_{\mathrm{c}}}^{\max p_{\mathrm{c}}}(g_{\mathrm{c}}-g_{\mathrm{l}})\,\mathrm{d}\,p_{\mathrm{c}}, \tag{8}$$

where $\min p_{\mathrm{c}}$ and $\max p_{\mathrm{c}}$ refer to the minimum and maximum pressures in the reservoir (p_{c}). Generally, the $\min p_{\mathrm{c}}$ and $\max p_{\mathrm{c}}$ are very close to the suction and discharge pressures, respectively.

The Gibbs free energy of helium gas is a function of state with temperature and pressure. Fig. 6 shows the relationship between the specific Gibbs free energy of helium and its pressure at T_0 (300 K), where the specific Gibbs free energy of helium is a monotonic and convex function of pressure. When the mass flow rate is fixed, the Gibbs free energy changes more at a lower pressure, indicating that a higher suction pressure of the rotary valve helps to decrease the viscosity exergy loss, based on Eqs. (7) and (8).

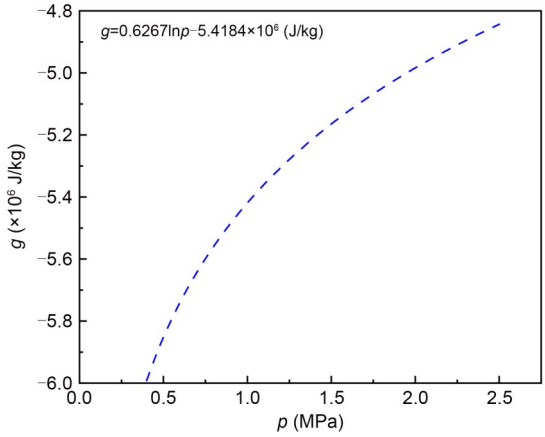

Fig. 6 Relationship between specific Gibbs free energy of helium and pressure at 300 K

Fig. 7 displays the ratio of $\dot{E}_{\mathrm{fric,d}}$ and $\dot{E}_{\mathrm{fric,s}}$ (Ψ) with different suction and discharge pressures. For a fixed discharge pressure of 2 MPa, as the suction pressure increases from 0.4 MPa to 1.8 MPa, Ψ increases from 0.60 to 0.95, leading to a lower $\dot{E}_{\mathrm{fric,s}}$ at a higher suction pressure. Therefore, increasing suction pressure can reduce the exergy loss at the suction valve.

2.3 Assessment of exergy loss generated in the rotary valve

After testing the leakage loss and viscosity loss in the rotary valve, we tested the distribution of $\dot{E}_{\mathrm{fric,d}}$, $\dot{E}_{\mathrm{fric,s}}$, and $\dot{E}_{\mathrm{leak}}$ generated in the rotary valve when two reservoirs with volumes of 0.5 L and 2.0 L were installed (Fig. 8). The mean pressure (p_{m}) during the test was constant at 1.7 MPa, and the operating frequencies were between 0.8 Hz and 2.6 Hz.

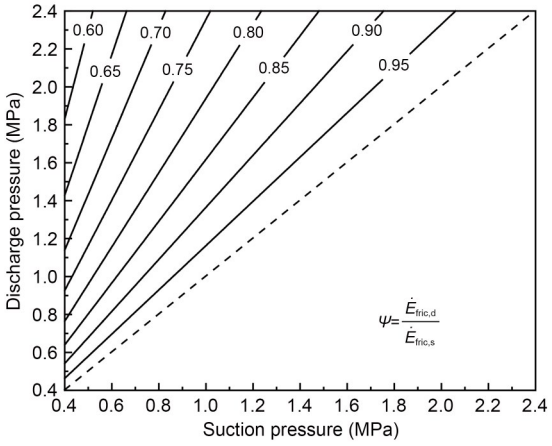

Fig. 7 Ratios of $\dot{E}_{\mathrm{fric,d}}$ and $\dot{E}_{\mathrm{fric,s}}$ with different suction and discharge pressures

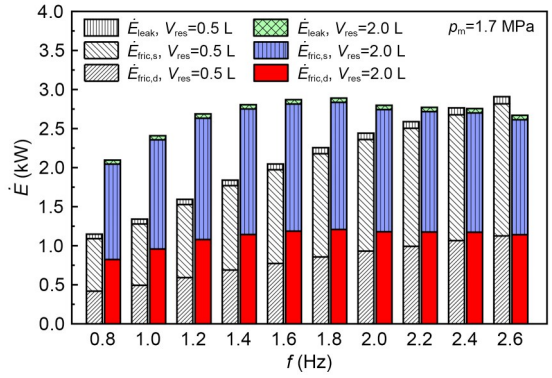

Fig. 8 Tested distribution of $\dot{E}_{\mathrm{fric,d}}$, $\dot{E}_{\mathrm{fric,s}}$, and $\dot{E}_{\mathrm{leak}}$ in the rotary valve using two reservoirs with volumes of 0.5 L and 2.0 L

As indicated in Fig. 8, the leakage loss was about 2.5% of the viscosity loss under all testing conditions, proving viscosity loss to be dominant in exergy loss at the rotary valve. Applying Eqs. (7) and (8) revealed that viscosity loss can be affected by the volume of the gas reservoir and the Gibbs free energy with different pressures. When the rotary valve is connected to a 0.5 L reservoir, the mass flow rate is small and increases linearly with the operating frequency, leading to a positive correlation of total exergy loss with operating frequency. When the rotary valve is connected to a 2.0 L reservoir, the mass flow rate is high and is limited by the flow area of the suction and discharge

valves in the rotary valve. Thus, exergy loss does not consistently increase with operating frequency. Compared to $\dot{E}_{\mathrm{fric,d}}$, $\dot{E}_{\mathrm{fric,s}}$ takes up a slightly larger portion of the exergy loss. Therefore, minimizing the flow resistance of the suction valve and discharge valve is essential to reduce exergy loss.

3 Structural optimization to reduce friction loss in rotary valves

Based on assessments of the exergy loss at the rotary valve and work done by Panda et al. (2019) and Xu et al. (2019), we recommend reducing the flow resistance of the suction valve and discharge valve to optimize the rotary valve. The original rotary valve (RV1) has a flow area of 40 mm^2. With the help of Sage, the changes in the cooling power of a two-stage GM-PTC with different flow areas of the rotary valve are presented in Fig. 9. More information about the two-stage GM-PTC can be found in Section 4.

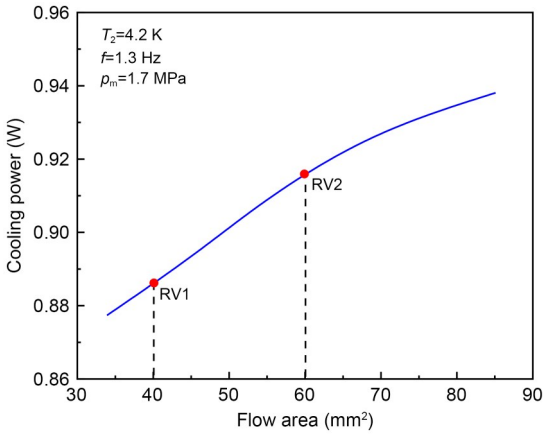

Fig. 9 Relationship between the flow area of the rotary valve and the cooling power of the GM-PTC at cooling temperature of 4.2 K as plotted by Sage (T_2 is the cooling temperature of the 2nd stage)

The figure shows that the cooling power at 4.2 K increases with the flow area of the rotary valve, indicating better performance with a larger flow area. However, because it is limited by the motor torque and 3D structure of the rotary valve, the flow area can only be expanded to 60 mm^2. Hence, we fabricated and tested an optimized rotary valve (RV2) that had a larger equivalent flow area than the original one, to validate the exergy loss assessment described in Section 2. RV1 is shown in Fig. 2, and RV2 in Fig. 10. Compared to RV1, the equivalent flow area of RV2 was about 1.5 times larger, with the same valve timing.

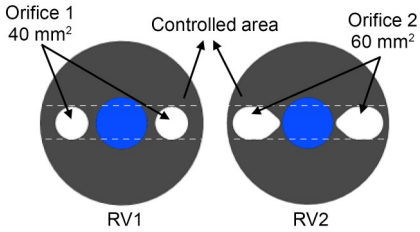

Fig. 10 Structure of the stators in both rotary valves (RV1 and RV2)

Based on the two experimental platforms illustrated in Section 2, we tested the suction pressure, discharge pressure, and mass flow rate of RV1 and RV2 with different mean pressures, when the rotary valve was connected to a gas reservoir (0.5 L or 2.0 L). Fig. 11 shows the suction pressure and discharge pressure results for RV1 and RV2. The dashed and solid lines in Fig. 11 present the suction and discharge pressures on both sides of the RV1 and RV2, respectively. It is worth noting in Fig. 11 that for a fixed frequency

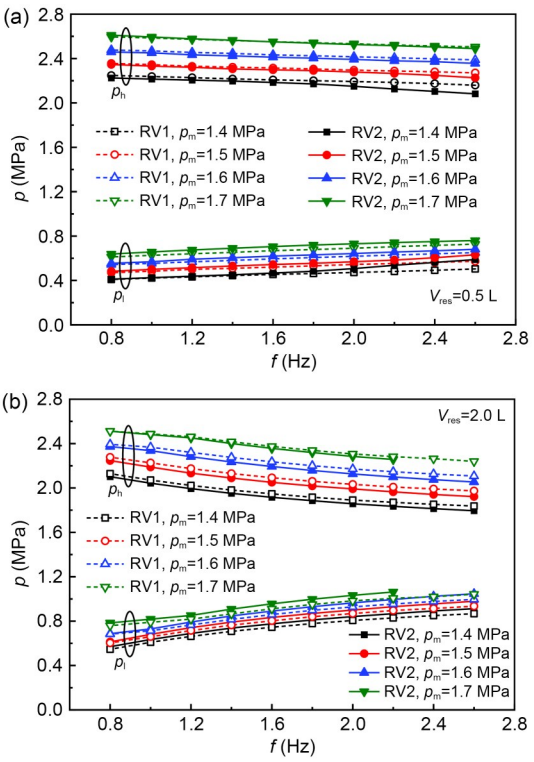

Fig. 11 Tested suction and discharge pressures of RV1 and RV2 with different mean pressures and frequencies and two gas reservoirs: (a) 0.5 L reservoir; (b) 2.0 L reservoir

and mean pressure, RV2 (solid line) obtained a lower high pressure (p_h) and a higher low pressure (p_l) than RV1 (dashed line). As a result, the pressure difference produced by RV2 was smaller than that produced by RV1, proving that RV2 had a lower flow resistance.

Fig. 12 shows the test results for the mass flow rates and leakage flow rates of RV1 and RV2. One can see that the leakage mass flow rates of the two rotary valves are very close. The maximum leakage mass flow rate was about 3% of the mass flow rate for both rotary valves. Thus, leakage loss can be neglected when assessing exergy loss in RV1 and RV2. When these values are used in Eq. (6), it becomes apparent that both the pressure-change rate and volume of the gas reservoir are linked to the tested mass flow rate.

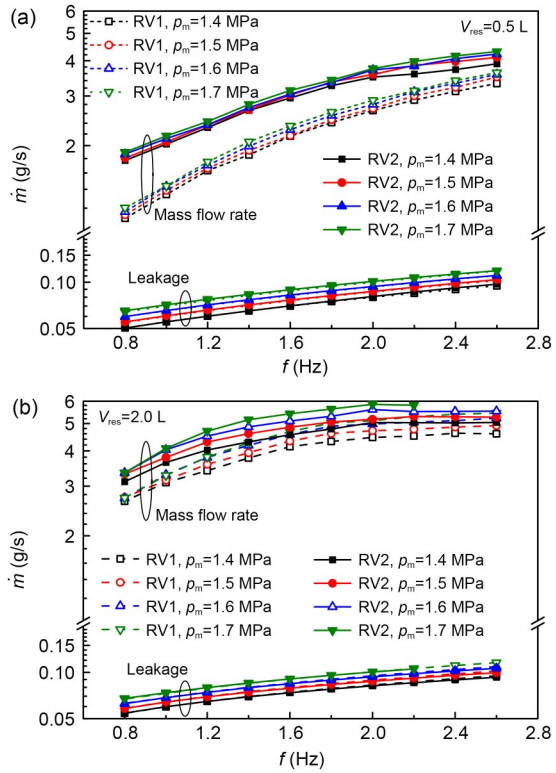

Fig. 12 Tested mass flow rate and leakage mass flow rate for RV1 and RV2 with two gas reservoirs: (a) 0.5 L reservoir; (b) 2.0 L reservoir

As shown in Fig. 12a, when the 0.5 L reservoir was connected to the rotary valves, the mass flow rate increased by up to 58% (from 1.2 g/s to 1.9 g/s at 0.8 Hz) after we replaced RV1 with RV2. For the 2.0 L reservoir (Fig. 12b), the mass flow rate increased by up to 26% (from 2.7 g/s to 3.4 g/s at 0.8 Hz) after RV2 was swapped in. Therefore, the mass flow rate increased for both gas reservoirs with RV2. The assessment of exergy loss in RV1 and RV2 is displayed in Fig. 13.

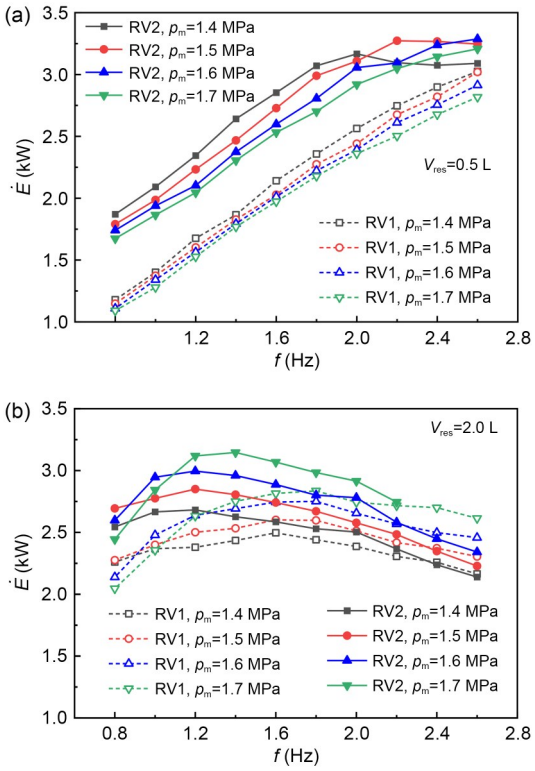

Fig. 13 Exergy loss in RV1 and RV2 with two gas reservoirs: (a) 0.5 L reservoir; (b) 2.0 L reservoir

It should be noted that during the RC load testing, we regarded the gas reservoir as a pure capacitive component without consuming work (Swift, 2002). Therefore, the exergy transferred by the compressor was dissipated in RV1 and RV2. Fig. 13a shows that RV2 dissipated up to 1.5 times more exergy than RV1 with the 0.5 L reservoir.

When the 2.0 L reservoir was connected to the rotary valves, the maximum exergy dissipated by RV2 was up to 1.2 times that dissipated by RV1, as shown in Fig. 13b. Therefore, the flow resistance in the rotary valve can be reduced by increasing the flow area, thus allowing more exergy to be delivered efficiently to the cold head by the rotary valve.

4 Experimental verification of exergy analysis upon a whole GM-PTC

Since we carried out the exergy-loss assessment of the rotary valves at ambient temperatures, we also

verified the feasibility of the structure optimization of RV2 in a complete GM-PTC. To validate the improvement brought by RV2 to the cooling performance of GM-PTCs, we connected a separated two-stage GM-PTC to the test platform shown in Fig. 5. The main geometric parameters of the GM-PTC are listed in Table 3, and a schematic diagram of the testing system is shown in Fig. 14.

Table 3 Geometrical parameters of the two-stage GM-PTC

Component	Dimension (matrix)
1st regenerator	Φ60.2 mm×200.5 mm (300# mesh screens SS304)
1st pulse tube	Φ46.0 mm×172.0 mm
2nd regenerator	Φ35.0 mm×185.0 mm (50% Pb+50% $HoCu_2$ (volume fraction))
2nd pulse tube	Φ27.4 mm×379.0 mm
1st/2nd reservoir	3.0 L

The testing system monitored the suction and discharge pressures (namely p_h and p_l) of the compressor, and the pressure of the load at the inlet of the cold head (p_c), with the same pressure gauges shown in Fig. 5. To calculate the output exergy of the compressor, we used a flowmeter to monitor its DC mass flow rate (Liu et al., 2017; Zhao et al., 2023). The performance of the GM-PTC was reflected by the cooling temperature and cooling power. Two Cernox thermometers and a Lakeshore 224 were used to monitor the cooling temperatures of the two cold heads of the GM-PTC. Two heating resistors were attached to the first- and second-stage cold heat exchangers to obtain the cooling power with a Keithley 2700 multimeter. Table 4 summarizes the information on the parameters measured on the test platform for a two-stage GM-PTC.

We tested the cooling performance of the two-stage GM-PTC connected to RV1 or RV2 rotary valves by using the same S603DH compressor. The mean pressure in the GM-PTC was 1.7 MPa, the operating

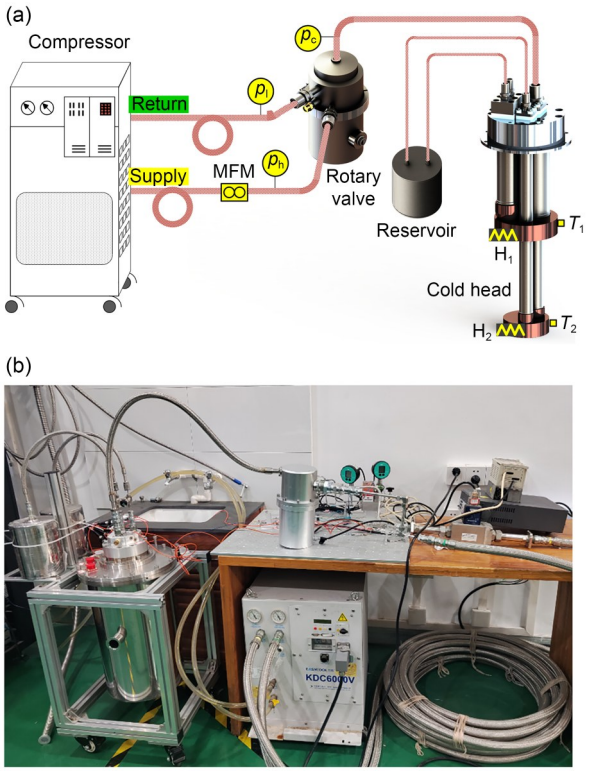

Fig. 14 Test platform of a two-stage GM-PTC: (a) schematic diagram; (b) photograph. T_1 is the cooling temperature of the 1st stage; H_1 is the heater of the 1st stage; H_2 is the heater of the 2nd stage; MFM is the mass flowmeter

frequency of RV1 and RV2 was fixed at 1.3 Hz, and the input electrical power of the compressor was maintained at 6 kW. Fig. 15a shows the temperature changes in the second-stage cold heat exchanger during the cool-down process of the GM-PTC when connected to an RV1 or RV2 rotary valve.

During the entire cool-down period, the second-stage cold heat exchanger was cooled to 2.55 K and 2.50 K with RV1 and RV2 installed, respectively. The cooling speed of the GM-PTC from ambient temperature to about 20 K was 7.2% faster with RV2 (4.18 K/min) than with RV1 (3.90 K/min). The cool-down period for the GM-PTC with RV1 from 20 K to 4.2 K is very close to the period with RV2.

Table 4 Information on the parameters measured on the test platform of a two-stage GM-PTC

Parameter	Symbol	Sensor	Range	Uncertainty
Electric power		DTSU5886	0–13.2 kW	±0.1 kW
Pressure oscillation	p_h, p_l, p_c	Keller M5HB	0–5.0 MPa	±5 kPa
Mass flow of compressor		TELEDYNE HFM305	0–8 g/s	±0.08 g/s
Cooling temperature	T_2	Cernox CX-1050-CU-HT-1.4L	1.4–325.0 K	±7.1 mK (at 4.2 K)
Cooling power		Keithley 2700 with a 50 Ω resistance	0–18 W	±5.5 mW

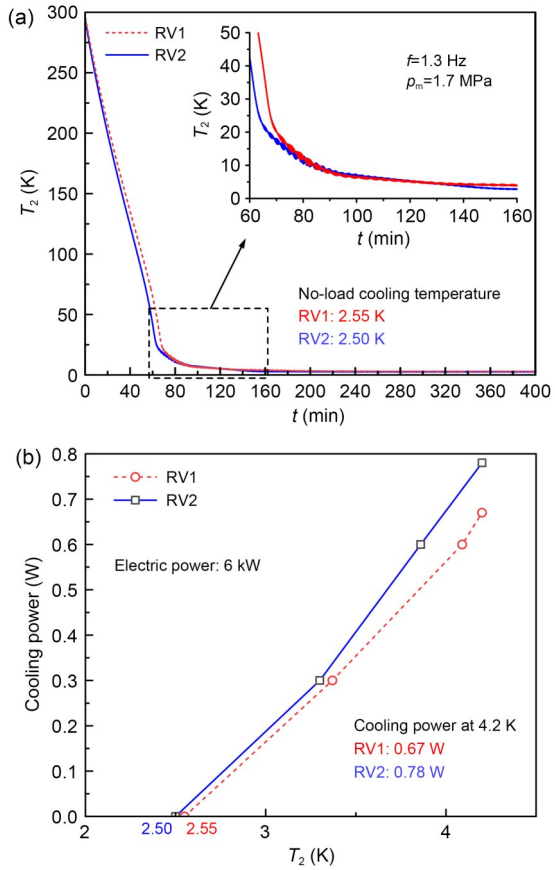

Fig. 15 Comparison of the cooling performance of a two-stage GM-PTC with an RV1 or RV2 rotary valve installed: (a) cool-down curve; (b) cooling power

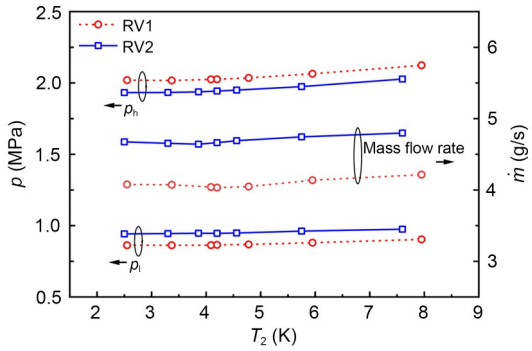

Fig. 16 Mass flow rate versus suction and discharge pressures with different cooling temperatures of the 2nd stage

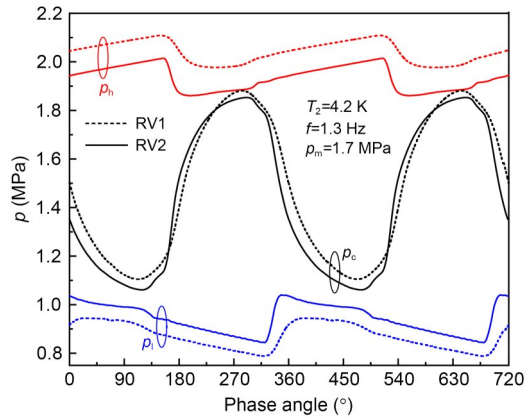

Fig. 17 Pressure variations in both rotary valves (RV1 and RV2) at a cooling temperature of 4.2 K (dashed lines: RV1; solid lines: RV2)

Fig. 15b shows that the cooling power changes with temperature when using RV1 or RV2 with the GM-PTC. The cooling power of the GM-PTC at 4.2 K was 0.67 W and 0.78 W with RV1 and RV2, respectively, indicating an improvement of 16.4% in cooling efficiency when using RV2 instead of RV1.

Fig. 16 shows the suction pressure, discharge pressure, and DC mass flow rate of the compressor with different cooling temperatures, using either RV1 or RV2. It can be seen from the figure that the installation of the RV2 rotary valve significantly reduced the difference between suction and discharge pressures and raised the suction pressure, leading to an increased DC mass flow rate of the compressor.

To reveal the alternating flow characteristics in RV1 and RV2, the pressure variations in the high-pressure chamber (p_h) and low-pressure chamber (p_l) and at the cold head (p_c) in one cycle, with a cooling temperature of 4.2 K, are displayed in Fig. 17. Compared to RV1, there was a smaller difference between the p_h and $\max p_c$, as well as between $\min p_c$ and p_l, during one cycle when RV2 was used. The reduction of the pressure difference indicates lower flow resistance in the rotary valve, which corresponds to higher efficiency (by 16%) of the GM-PTC. As a result, increasing the flow area helps to lower the exergy loss generated in the rotary valve and produces better performance for the GM-PTC at liquid helium temperatures. However, it was difficult to assess the exergy loss test in the cold head since the amplitude and phase relationships between the alternating mass flow rate and pressure were hard to monitor without the addition of numerical simulation.

5 Conclusions

To improve the cooling efficiency of GM-PTCs at 4.2 K, we conducted structural optimization of the

rotary valve by assessing the exergy loss, and verified the optimization by experimental testing. We used an experimental test method to assess the exergy loss (consisting of leakage loss and viscosity loss) in the rotary valve and conducted it on two experimental platforms. The results show that the leakage loss is less than 2.5% of the total exergy loss and the viscosity loss accounts for more than 97.5% of the total exergy loss, indicating that reduction of flow resistance in the rotary valve is essential to lower exergy loss. With the help of the exergy-loss assessment results, we chose an optimized rotary valve (RV2) with 1.5 times the flow area of the original one (RV1) to analyze the exergy loss. The maximum exergy transferred from the compressor to the load side by RV2 is 1.5 times that transferred by RV1. Finally, we conducted a test of the cooling performance of a remote two-stage GM-PTC which had either the optimized rotary valve (RV2) or the original one (RV1) installed, to further validate the exergy-loss assessment of the rotary valves. The results show that when the input power of the compressor is 6 kW, the GM-PTC provides a cooling power of 0.78 W at 4.2 K when replacing RV1 with RV2, which leads to an improvement of 16.4% in the cooling efficiency of the GM-PTC.

Acknowledgments

This work is supported by the National Key Research & Development Program of China (No. 2023YFF0721304) and the Key Research & Development Program of Jiangsu Province (No. 2021015-4), China.

Author contributions

Qinyu ZHAO and Ruize LI designed the research. Yanrui ZHANG and Jun CHENG processed the corresponding data. Qinyu ZHAO and Haoren WANG wrote the first draft of the manuscript. Bo WANG helped to organize the manuscript. Bo WANG, Hua ZHANG, and Zhihua GAN revised and edited the final version.

Conflict of interest

Qinyu ZHAO, Jun CHENG, Yanrui ZHANG, Haoren WANG, Bo WANG, Ruize LI, Hua ZHANG, and Zhihua GAN declare that they have no conflict of interest.

References

Alduino C, Alessandria F, Balata M, et al., 2019. The CUORE cryostat: an infrastructure for rare event searches at millikelvin temperatures. *Cryogenics*, 102:43-56. https://doi.org/10.1016/j.cryogenics.2019.06.011

Bluefors, 2023a. Cryomech PT425 Pulse Tube Cryocooler. Bluefors. https://bluefors.com/products/cryomech-products/pt425-pulse-tube-cryocooler/

Bluefors, 2023b. Cryomech PT450 Pulse Tube Cryocooler. Bluefors. https://bluefors.com/products/pulse-tube-cryocoolers/pt450/

Choi CQ, 2022. IBM Unveils 433-Qubit Osprey Chip. IEEE Spectrum. https://spectrum.ieee.org/ibm-quantum-computer-osprey

de Waele ATAM, 2011. Basic operation of cryocoolers and related thermal machines. *Journal of Low Temperature Physics*, 164(5):179-236. https://doi.org/10.1007/s10909-011-0373-x

de Waele ATAM, 2012. Finite heat-capacity effects in regenerators. *Cryogenics*, 52(1):1-7. https://doi.org/10.1016/j.cryogenics.2011.09.015

Gan ZH, Dong WQ, Qiu LM, et al., 2009. A single-stage GM-type pulse tube cryocooler operating at 10.6 K. *Cryogenics*, 49(5):198-201. https://doi.org/10.1016/j.cryogenics.2009.01.004

Gedeon D, 2014. Sage User's Guide. Sage Version 10th Edition. Gedeon Associates, USA.

Hao XH, Cosco J, Zerkle B, et al., 2022. Development of high cooling capacity and high efficiency 4.2 K pulse tube cryocoolers. International Cryocooler Conference, p.235-240.

Hitachi, 2023. Cryogenic. Johnson Controls-Hitachi Air Conditioning Company. https://compressors.hitachiaircon.com/en/ranges/scroll-compressor/cryogenic

Hollister MI, Dhuley RC, James C, et al., 2023. An update on the Colossus mK platform at Fermilab. *IOP Conference Series: Materials Science and Engineering*, 1302:012030. https://doi.org/10.1088/1757-899X/1302/1/012030

Ji ZQ, Fan J, Dong J, et al., 2022. Development of a cryogen-free dilution refrigerator. *Chinese Physics B*, 31(12):120703. https://doi.org/10.1088/1674-1056/ac9042

Karpenko M, Bogdevičius M, 2020. Investigation of hydrodynamic processes in the system–"pipeline-fittings". TRANSBALTICA XI: Transportation Science and Technology, p.331-340. https://doi.org/10.1007/978-3-030-38666-5_35

Karpenko M, Stosiak M, Šukevičius Š, et al., 2023. Hydrodynamic processes in angular fitting connections of a transport machine's hydraulic drive. *Machines*, 11(3):355. https://doi.org/10.3390/machines11030355

Kasai J, Koyama T, Yokota M, et al., 2022. Development of a near-5-Kelvin, cryogen-free, pulse-tube refrigerator-based scanning probe microscope. *Review of Scientific Instruments*, 93(4):043711. https://doi.org/10.1063/5.0084888

Lei T, Xu MY, 2022. Development of a 2 W 4 K pulse tube refrigerator with remote valve. International Cryocooler Conference, p.241-247.

Liang W, de Waele ATAM, 2007. A new type of streaming in pulse tubes. *Cryogenics*, 47(9-10):468-473. https://doi.org/10.1016/j.cryogenics.2007.04.005

Liu DL, Dietrich M, Thummes G, et al., 2017. Numerical simulation of a GM-type pulse tube cryocooler system: part II. Rotary valve and cold head. *Cryogenics*, 81:100-106. https://doi.org/10.1016/j.cryogenics.2016.11.006

Panda D, Satapathy AK, Sarangi SK, 2019. Effect of valve opening shapes on the performance of a single-stage Gifford-McMahon cryocooler. *Engineering Reports*, 1(3): e12044. https://doi.org/10.1002/eng2.12044

Qiu LM, Thummes G, 2002. Valve timing effect on the cooling performance of a 4 K pulse tube cooler. *Cryogenics*, 42(5): 327-333. https://doi.org/10.1016/S0011-2275(02)00043-7

Radebaugh R, O'Gallagher A, Gary J, 2002. Regenerator behavior at 4 K: effect of volume and porosity. *AIP Conference Proceedings*, 613(1):961-968. https://doi.org/10.1063/1.1472117

SHI Cryogenics Group, 2023. Two-Stage Gifford-McMahon Cryocoolers. SHI Cryogenics Group. https://shicryogenics.com/products/cryocoolers/

Swift GW, 2002. Thermoacoustics: a Unifying Perspective for Some Engines and Refrigerators. Acoustical Society of America, New York, USA, p.97-106.

Tanaeva IA, Bos CGK, de Waele ATAM, 2006. High-frequency pulse-tube refrigerator for 4 K. *AIP Conference Proceedings*, 823(1):821-828. https://doi.org/10.1063/1.2202491

The CUORE Collaboration, 2022. Search for Majorana neutrinos exploiting millikelvin cryogenics with CUORE. *Nature*, 604(7904):53-58. https://doi.org/10.1038/s41586-022-04497-4

Thummes G, Giebeler F, Heiden C, 1995. Effect of pressure wave form on pulse tube refrigerator performance. *In*: Ross RG (Ed.), Cryocoolers 8. Springer, Boston, USA, p.383-393. https://doi.org/10.1007/978-1-4757-9888-3_39

Wang B, Gan ZH, 2013. A critical review of liquid helium temperature high frequency pulse tube cryocoolers for space applications. *Progress in Aerospace Sciences*, 61: 43-70. https://doi.org/10.1016/j.paerosci.2013.05.001

Wang C, Qiu LM, Dong WQ, et al., 2010. Comparison test of rotary valve system and solenoid valves system for a G-M type pulse tube cryocooler. *Cryogenics*, (5):6-10 (in Chinese). https://doi.org/10.3969/j.issn.1000-6516.2010.05.002

Xu MY, Morie T, Bao Q, 2019. Cryocooler and Rotary Valve Mechanism. US Patent 10371417B2.

Zhao QY, Wang B, Chao W, et al., 2023. Numerical simulation and exergy analysis of a single-stage GM cryocooler. *Heliyon*, 9(7):e18479. https://doi.org/10.1016/j.heliyon.2023.e18479

Zhou SL, Matsubara Y, 1998. Experimental research of thermoacoustic prime mover. *Cryogenics*, 38(8):813-822. https://doi.org/10.1016/S0011-2275(98)00055-1

Zhu SW, Kakimi Y, Matsubara Y, 1997. Investigation of active-buffer pulse tube refrigerator. *Cryogenics*, 37(8):461-471. https://doi.org/10.1016/S0011-2275(97)00080-5

Zhu SW, Kakimi Y, Matsubara Y, 1998. Waiting time effect of a GM type orifice pulse tube refrigerator. *Cryogenics*, 38(6):619-624. https://doi.org/10.1016/S0011-2275(98)00026-5

Zhu SW, Nogawa M, Inoue T, 2009. Analysis of DC gas flow in GM type double inlet pulse tube refrigerators. *Cryogenics*, 49(2):66-71. https://doi.org/10.1016/j.cryogenics.2008.10.003